Available online at www.sciencedirect.com

ScienceDirect

Journal of Materiomics 1 (2015) 33–44

www.ceramsoc.com/en/

www.journals.elsevier.com/journal-of-materiomics/

Two-dimensional MoS_2: Properties, preparation, and applications

Xiao Li [a,b], Hongwei Zhu [a,b,*]

[a] School of Materials Science and Engineering, State Key Laboratory of New Ceramics and Fine Processing, Tsinghua University, Beijing 100084, China
[b] Center for Nano and Micro Mechanics (CNMM), Tsinghua University, Beijing 100084, China

Received 26 December 2014; revised 14 January 2015; accepted 30 January 2015
Available online 1 April 2015

Abstract

Graphene-like two-dimensional (2D) transition metal dichalcogenides (TMDCs) have been attracting a wide range of research interests. Molybdenum disulfide (MoS_2) is one of the most typical TMDCs. Its particular direct band gap of 1.8 eV in monolayer and layer dependence of band structure tackle the gapless problems of graphene, thus making it scientific and industrial importance. In this Review, we attempt to provide the latest development of optical and electronic properties, synthesis approaches, and potential applications of 2D MoS_2. A roadmap towards fabricating hybrid structures based on MoS_2 and graphene is highlighted, proposing ways to enhance properties of the individual component and broaden the range of functional applications in various fields, including flexible electronics, energy storage and harvesting as well as electrochemical catalysis.

Keywords: Two-dimensional; Transition metal dichalcogenides; Molybdenum disulfide; Chemical vapor deposition; van der Waals heterostructure

1. Introduction

Graphene, which is a typical two-dimensional (2D) layered material, has experienced its brilliant age since it was first mechanically exfoliated from three-dimensional (3D) graphite in 2004 [1]. Many strikingly highlighted properties, such as its high transparency (97.7% transmittance in the visible spectrum), high thermal conductivity at room temperature (3×10^3 W/m K), high electrical conductivity (~$10^4\ \Omega^{-1}\ cm^{-1}$), high Young's modulus (1.1 TPa) and high specific surface area (2630 m^2/g) have been identified in monolayer graphene [2,3]. All these extraordinary properties benefit graphene for various applications, including transparent electrodes [4], energy storage [5], solar cells [6,7], wearable devices [8] and catalysis [9]. Graphene is defined as a semi-metallic material because of its special π−π* band structure. The conduction band and valence band are symmetrical about Dirac point, so its electronic properties near K point can be described with Dirac equation, not Schrodinger equation. The Fermi surface is just the intersection point of the conduction band and valence band, making graphene to be a zero gap material [1]. This unique structure gives graphene extremely outstanding electrical property, while limits its applications in logical circuits for low-power electronic switching.

Recently, researchers have been refocusing on other graphene-like 2D materials, aiming at overcoming the shortage of graphene and broadening its range of applications [10,11]. 3D bulk materials possess similar traits to obtain their corresponding 2D layered materials [12]. The melting temperature of these materials is higher than 1000 °C, and they should be both chemically inert and surface stable at room temperature. Generally, 2D insulating and semiconducting materials are more likely to be obtained due to the intrinsic chemical activity of most metallic materials. Graphite, hBN and molybdenum disulfide (MoS_2) stand out in this

* Corresponding author. School of Materials Science and Engineering, State Key Laboratory of New Ceramics and Fine Processing, Tsinghua University, Beijing 100084, China.
E-mail address: hongweizhu@tsinghua.edu.cn (H. Zhu).
Peer review under responsibility of The Chinese Ceramic Society.

http://dx.doi.org/10.1016/j.jmat.2015.03.003

competition, which are all widely used as lubricants at first. hBN is electrical insulator and widely used as gate dielectrics in capacitors [13]. Due to the widespread in nature as molybdenite, MoS_2 has been one of the most studied layered transition metal dichalcogenides (TMDCs). Monolayer MoS_2 is a semiconductor with a direct bandgap of 1.8 eV [10]. This property of MoS_2 is inspiring, which will largely compensate the weakness of gapless graphene, thus making it possible for 2D materials to be used in the next generation switching and optoelectronic devices. Thus far, MoS_2 has achieved primary progress in the following fields, including energy conversion [14] and storage [15] and hydrogen evolution reaction (HER) [16]. Additionally, MoS_2 with odd number of layers could produce oscillating piezoelectric voltage and current outputs, indicating its potential applications in powering nanodevices and stretchable electronics [17].

In this Review, taking MoS_2 as a benchmark material, we attempt to give a basic outlook of the large family of 2D TMDCs, highlighting their interesting physical properties that are most relevant in device applications and systematically introducing the recent process in the preparation methods, including exfoliation and chemical vapor deposition (CVD). Finally we delineate and categorize a series of emerging applications of MoS_2, such as field-effect transistors (FETs), memory devices, photodetectors, solar cells, electrocatalysts for HER, and lithium ion batteries.

2. Properties

TMDCs, whose generalized formula is MX_2 (M = Transition metal (Ti, Zr, Hf, V, Nb, Ta, Mo, W, Tc, Re, Co, Rh, Ir, Ni, Pd, Pt), X = Chalcogen (S, Se, Te)), have a large family of materials and their electronic characters could be semiconducting, metallic and superconducting [12]. We focus on the most widely and stable existing semiconducting MoS_2 for introduction. In the single layer of MoS_2 films, Mo (+4) and S (−2) are arranged to a sandwich structure by covalent bonds in a sequence of S−Mo−S [18], whereas the sandwich layers are interacted by relatively weak van der Waals forces (Fig. 1a). Generally, each layer has a thickness of ~0.65 nm. Monolayer MoS_2 with trigonal prismatic polytype is found to be semiconducting (referred to as 2H), while that with octahedral crystal symmetry configuration (referred to as 1T) is metallic (Fig. 1b) [19]. Very similarly to graphene, MoS_2 is mechanically flexible with a Young's modulus of 0.33 ± 0.07 TPa [20].

2.1. Raman spectra

Raman spectra is a convenient characterization method to illustrate the evolution of structural parameters in layered materials in changing from the 3D bulk blocks to the 2D van der Waals bonded constructions, which has been popularly used to study the quality and layer number of graphene. Similarly, early in 2010, Changgu Lee's group has been systematically characterized single- and few-layer MoS_2 by Raman spectra [21]. Generally, two typical Raman peak, E^1_{2g} and A_{1g} are investigated to reflect the crystal structure of MoS_2. E^1_{2g} and A_{1g} are indicators of in-plane and out-of-plane vibration modes of S atoms, respectively (Fig. 1c) [21]. From bulk to monolayer, three changing rules are collected. First, E^1_{2g} exhibits a regularly blue-shifted while A_{1g} shows an opposite red-shifted. E^1_{2g} and A_{1g} locate at the ~384 cm^{-1} and 405 cm^{-1} for single layer MoS_2 (Fig. 1d, f). Second, the peak frequency difference between E^1_{2g} and A_{1g} shows a clear decreasing trend as a function of layer number (Fig. 1d, f) [21]. The frequency spacing is about 25 cm^{-1} and 19 cm^{-1} for bulk and monolayer MoS_2, respectively. Third, two peak intensities almost increase linearly up to four layers with increasing layer thickness, while decrease for thicker MoS_2 (Fig. 1e) [21]. Yongjie Zhan's group has also reported the intensity ratio between E^1_{2g} and silicon (Si) substrate is

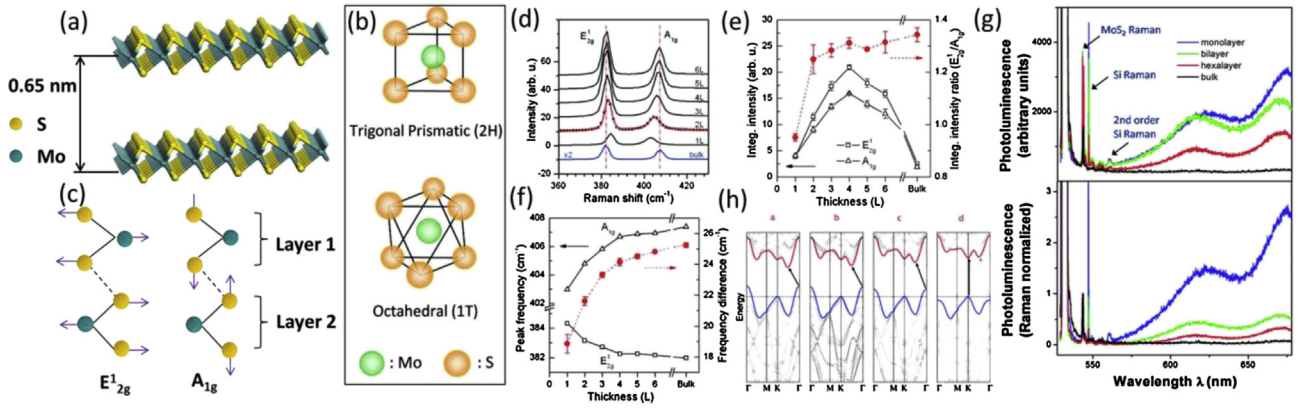

Fig. 1. Crystal structure and optical properties of MoS_2. (a) Chemical structure of two layers of MoS_2. (b) Two polytypes of single layer MoS_2: trigonal prismatic (1H) and octahedral (1T). (c) Schematic illustrations of the two typical Raman-active phonon modes (E^1_{2g}, A_{1g}). (d) Raman spectra of thin (nL) and bulk MoS_2 films. (e) Frequencies of E^1_{2g} and A_{1g} Raman modes (left vertical axis) and their difference (right vertical axis) corresponding to layer thickness. (f) Thickness dependence of integrated intensity (left vertical axis) and ratio of integrated intensity (right vertical axis) for the two Raman modes. (g) PL and Raman spectra of MoS_2 monolayer, bilayer, hexalayer, and bulk sample. (h) Calculated band structures of bulk MoS_2, quadrilayer MoS_2, bilayer MoS_2, and monolayer MoS_2 (from left to right, a~d). The solid arrows indicate the lowest energy transitions. Panel b reprinted with permission from Ref. [19]. Copyright 2011 American Chemical Society. Panel a, c ~ f reproduced and reprinted with permission from Ref. [21]. Copyright 2010 American Chemical Society. Panel g, h reprinted with permission from Ref. [23]. Copyright 2010 American Chemical Society.

associated with layer thickness, ~0.05 and 0.09 for single- and double-layer samples [22].

2.2. Photoluminescence (PL) evolution and band structure engineering

PL spectra are found to be closely related to the number of layers in MoS_2 [19]. Andrea Splendiani' group has reported the distinct PL difference between monolayer (1L), bilayer (2L), quadrilayer (4L) and hexalayer (6L) samples (Fig. 1g) [23]. Two evident absoption peaks at 670 nm and 627 nm, identified as A1 and B1 excitons, can be observed in the spectrum for 1L MoS_2, while they both disappear in bulk MoS_2. These two excitons are associated with the energy split from valence band spin-orbital coupling. Prominent resonances in 1L sample indicate the direct excitonic transitions at the Brillouin zone K point, which is also consistent with the theoretical prediction of indirect (1.2 eV) to direct (1.8 eV) bandgap transition in changing from bulk to single layer MoS_2. Thus, MoS_2 with its layer number varying from multilayer to monolayer, will lead to qualitatively change in its band structure, further explaining the prominent PL effect in 1L sample (Fig. 1h) [23].

2.3. Electrical performance

Single layer MoS_2 has a large direct bandgap of 1.8 eV, being suitable acting as switching nanodevices. In 2011, B. Radisavljevic's group proposed a single-layer MoS_2 transistor adopting a halfnium oxide as the gate dielectric material, in which the mobility of MoS_2 could be up to 200 $cm^2/(V\ s)$ at room temperature with the current on/off ratio to be 1×10^8 (Fig. 2a, b) [24]. Generally, MoS_2 based transistors show the n-type behavior. Later in 2012, Zongyou Yin's group reported a phototransistor based on the mechanically exfoliated single-layer MoS_2 for the first time (Fig. 2c) [25]. The switching character of this device is outstanding, with photocurrent generation and annihilation within only 50 ms (Fig. 2d) [25]. Under incident light control, the photoresponsivity could reach 7.5 mA/W at a gate voltage of ~50 V, much higher than that in graphene based devices (~1 mA/W at the gate voltage of 60 V) (Fig. 2e) [25]. This advantage gives MoS_2 best chances for

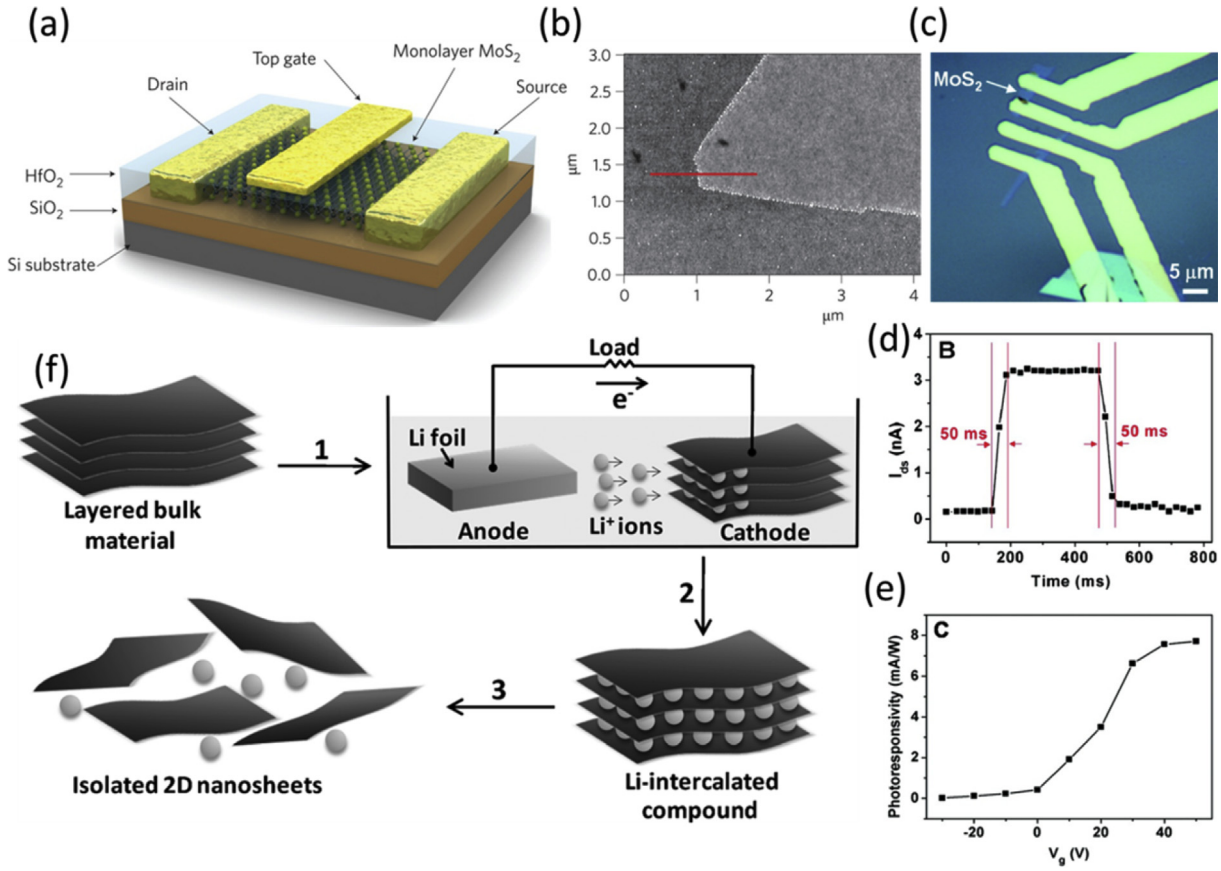

Fig. 2. Electrical performance of MoS_2 and its chemical exfoliation. (a) 3D schematic view of MoS_2 monolayer transistors. (b) AFM image of a single layer of MoS_2. Red line goes across the edge of MoS_2 to the Si substrate with a 270-nm-thick oxide layer. (c) Optical image of FET device made by single-layer MoS_2. (d) Photoswitching rate of on/off behavior of single-layer MoS_2 phototransistor at $V_{ds} = 1$ V, $P_{light} = 80$ μW. (e) Dependence of photoresponsivity on the gate voltage ($V_{ds} = 1$ V, Plight = 80 μW). (f) Electrochemical lithiation process for the fabrication of 2D nanosheets from the layered bulk material. Panel a, b reprinted with permission from ref 24. Copyright 2011, Rights Managed by Nature Publishing Group. Panel c ~ e reprinted with permission from ref 25. Copyright 2012 American Chemical Society. Panel f reprinted with permission from ref 28. Copyright 2011 WILEY-VCH Verlag GmbH & Co. KGaA, Weinheim.

future applications in many fields, including transistors, photodetectors and memory devices, broadening 2D graphene and graphene-like flexible materials into both transparent conducting and semiconducting areas.

3. Preparation

3.1. Exfoliation

Graphene's successful exfoliation from bulk graphite paves way for the fabrication of other graphene-like 2D materials [26] through the simple "Scotch tape method" [1]. Due to high quality monolayers occurring from mechanical exfoliation, this method is popularly used for intrinsic sheet production and fundamental research [24]. Nevertheless, this method is not suitable for practical applications on a large scale due to its low yield and disadvantages in controlling sheet size and layer number. In 2012, Karim Gacem's group proposed a general technique for fabricating high quality 2D layered materials, which was called anodic bonding. Sizes of few-layer MoS_2 obtained were relatively controllable and larger, ranging from 10 μm to several hundred microns [27].

Another class of exfoliation method is through chemical approach, including ion intercalation and solvent-based exfoliation [10]. In 2011, Hua Zhang's group reported a fast and highly-controllable method to exfoliate a series of semiconducting nanosheets. Through an electrochemical lithiation discharge process, bulk MoS_2 could be realized lithium intercalation (Fig. 2f) [28]. Then after subsequent ultrasonication, a high yield (92%) single-layer MoS_2 was achieved. Metallic 1T-MoS_2 accounted for a large proportion fabricated through the above way. Solvent-based exfoliation, also called Coleman method [29], was first reported in 2011, which could obtain mostly semiconducting 2H−MoS_2 from exfoliating suspended bulk MoS_2 flakes in organic solvents. O'Neill et al. further optimized this method by carefully controlling the sonication time, resulting in higher reported flake concentration of about 40 mg/mL and relatively increasing flake size [30]. Chemical exfoliation could largely increase production than mechanical exfoliation, whereas sonication during this process would cause defects to 2D lattice structure and reduce flake size down to a few thousand nanometers, limiting the applications of 2D nanosheets in the field of large-scale integrated circuits and electronic devices.

3.2. CVD synthesis

Recently, controllable preparation of 2D TMDCs with large-area uniformity has remained a big challenge. CVD approach has attracted widely attention because it could synthesis 2D TMDCs on a wafer-scale, which shows great potential toward practical applications like large-scale integrated electronics. This method not only could prepare continuous single film with certain thickness, but highlight in directly growth layered heterostructures, which would largely avoid interfacial contamination introduced during layer by layer transfer process. This part gives a systematical presentation of CVD synthesis of monolayer- or few-layer MoS_2. Typically, the following precursors are used to prepare MoS_2 film, including Mo based compound powder [31,32], deposited molybdenum (Mo) based film [22,33], ammonium thiomolybdates ($(NH_4)_2MoS_4$) film [34] and MoS_2 powder [35].

3.2.1. Sulfurization of Mo based compound

In 2012, for the first time, Lain-Jong Li's group reported a CVD method to synthesis large-area, monolayer MoS_2 films on silicon dioxide (SiO_2) substrate in ambient environment. Molybdenum trioxide (MoO_3) and sulfur (S) powders acted as solid reactants and SiO_2 substrate should be pretreated by graphene-like molecules to increase nucleation points (Fig. 3a) [31]. AFM cross-sectional profile characterization illustrates the thickness of MoS_2 layer is about 0.72 nm, very close to that of mechanically exfoliated single layer. FET based on this film shows typical n-type behavior and the current on/off ratio could reach up to 10^4 [31]. Later in 2013, Yifei Yu's group proposed a self-limiting CVD method under a pressure around 2 Torr to prepare uniform MoS_2 films of centimeters by changing MoO_3 to molybdenum chloride ($MoCl_5$) as precursors [32]. FET devices based on this high quality film show comparable performance to that reported by Li's group, the field-effect mobility of which could reach up to 0.03 $cm^2/(V\ s)$ [32].

3.2.2. Sulfurization of Mo and Mo based oxides

To further improve the uniformity in large areas, Yongjie Zhan's group pre-deposited a thin layer of Mo (~1−5 nm) on SiO_2 by e-beam evaporation, and then this substrate was placed in a tube furnace to react with sulfur vapor at 750 °C (Fig. 3b) [22]. The resulted samples were bi- or tri-layered in thickness with the interlayer spacing to be ~6.6 ± 0.2 Å. X-ray photoelectron spectroscopy (XPS) results illustrated that the ratio of Mo and S was nearly 1:2. Electrical measurements confirmed that the as-prepared MoS_2 showed resistor-like behavior, whose sheet resistance and typical mobility were within the range of 1.46×10^4−2.84×10^4 Ω/□ and 0.004−0.04 $cm^2/(V\ s)$, respectively [22]. Lain-Jong Li's group further adopted the similar way to thermally deposit MoO_3 thin films on the sapphire substrate. After two-step thermal reaction, MoO_3 was successfully sulfurized to be MoS_2 with few layers [33]. Atomic force microscopy (AFM) proved the thickness of the MoS_2 film was about 2 nm. Samples were transferred onto arbitrary substrates in wafer-scale by the general PMMA-assisted etching technique. To characterize the electrical performance of MoS_2 films, a bottom-gate FET device was constructed, which showed typical n-type behavior with electron mobility to be ~0.8 $cm^2/(V\ s)$ and on/off current ratio ~10^5 [33].

3.2.3. Thermal decomposition of $(NH_4)_2MoS_4$

Another effective approach to synthesis MoS_2 films in wafer scale with high controllability was through simple thermolysis of $(NH_4)_2MoS_4$. Keng-Ku Liu's group reported to have prepared bi- or trilayer continuous films on insulating substrates through this method (Fig. 3c) [34]. It was also

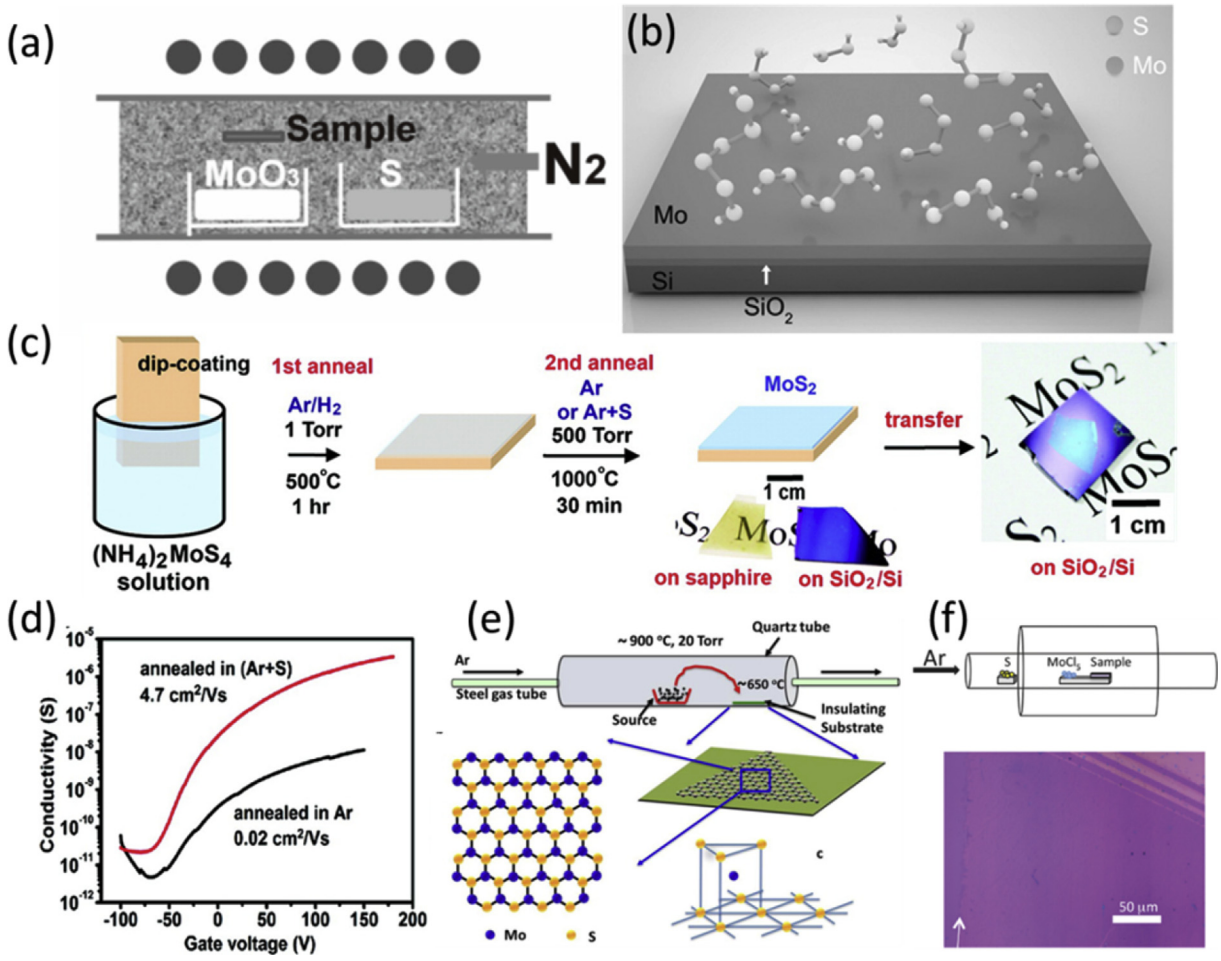

Fig. 3. General CVD preparation of MoS_2. (a) Sulfurization of MoO_3 powder. (b) Sulfurization of Mo films. (c) Schematic illustration of the two-step thermal decomposition of $(NH_4)_2MoS_4$. (d) The typical transfer curves (conductivity vs gate voltage V_g) for the devices fabricated using the MoS_2 trilayers annealed with and without sulfur according to methods displayed in (c). (e) Vapor-solid growth from MoS_2 powder. Panel a reprinted with permission from Ref. [31]. Copyright 2012 WILEY-VCH Verlag GmbH & Co. KGaA, Weinheim. Panel b reprinted with permission from ref 22. Copyright 2012 WILEY-VCH Verlag GmbH & Co. KGaA, Weinheim. Panel c, d reprinted with permission from Ref. [34]. Copyright 2012 American Chemical Society. Panel e reprinted with permission from Ref. [35]. Copyright 2013 American Chemical Society. Panel f reprinted with permission from Ref. 39. Copyright 2014 WILEY-VCH Verlag GmbH & Co. KGaA, Weinheim.

confirmed that the second-step high temperature sulfurization process could improve the crystallization to a large extent. The as-grown samples showed extremely high electrical performance (Fig. 3d), and bottom gate transistors fabricated with these films exhibited outstanding field-effect electron mobility as high as 4.7 $cm^2/(V\ s)$, exceeding previous reports [34]. One key and conclusive factor which must be carefully controlled is to achieve homogeneous dip-coated precursor films on target substrates.

3.2.4. Vapor-solid growth from MoS_2 powder

One particular and straightforward synthesis method needs to be mentioned was proposed by Sanfeng Wu and his co-workers in 2013, based on a vapor-solid growth mechanism, demonstrating the preparation of monolayer MoS_2 films on various insulating substrates (Fig. 3e) [35]. As-grown flakes were about 25 μm in dimension, with a maximum of ~35% at ~1.92 eV exhibiting substantial PL polarization at room temperature, which was comparable to that of samples prepared by mechanical exfoliation (~40% at 300 K) [35]. The limitation of this method lied on the random nucleation of MoS_2 crystals, leading to the presence of thicker zones and influencing the uniformity of samples.

3.2.5. Direct synthesis of graphene/MoS_2 composites

The intensive study and prosperous achievements on graphene paved the way for the development of other 2D graphene-like materials. Building van der Waals heterostructures based on these 2D blocks seems to be a leading research topic in recent years [12]. Evidently, layer-by-layer stacking is one of the most simple and straightforward methods for heterostructures construction. However, interfacial contamination would be an important factor to be considered. How to reduce adsorbates on individual layer and improve interface bonding becomes a bottleneck. Insulating substrates, such as SiO_2, Mica or sapphire, are always used for

MoS_2 preparation [31,34,44]. Recent studies show that graphene itself can be a suitable substrate for MoS_2 growth. Yumeng Shi and his coworkers presented a method to prepare MoS_2/graphene heterostructures bonded van der Waals force. MoS_2 nanoflakes on the graphene surface were hexagonal, with crystal size ranging from several hundred nanometers to several micrometers [36]. Although there existed a little lattice mismatch between graphene and MoS_2, the gap could be well accommodated within these heterostructures. The excellent conductivity of graphene combined with the good catalytic property of MoS_2 paves way to develop a second generation of graphene based nanostructures into a new era. In addition, MoS_2 films have the ambition to tackle the gapless problems of graphene. Hence, making full use of their particular advantages would largely enhance properties of the hybrid structures, broadening the range of applications in foreseen electronic, optoelectronic, catalytic and even energy storage fields. Following this trend and concept [37], continuous MoS_2 films of varying thickness on epitaxial graphene was prepared by Yu-Chuan Lin's group [38]. Very recently, Kathleen M. McCreary's group reported a relatively continuous and uniform MoS_2 single-layer films grown on large-area graphene, and the size of MoS_2/graphene heterostructures could be centimeters, making this type of structures more practical and controllable (Fig. 3f) [39]. In addition, Table 1 provides a systematic summary of the CVD preparation of MoS_2 not mentioned above [40].

4. Applications

Due to the particular optical and electrical performance of TMDCs, these 2D graphene-like has aroused expanding interest until now. As one of the most typical existing TMDCs, MoS_2 itself has evolved into a vast studying topic, gradually finding its applications in many related areas, such as transistors [24], photodetectors [48], solar cells [14], *etc*. However, due to the limitations in intrinsic structures, one simple material is highly difficult to satisfy all basic properties and functional performance in practical applications. For instance, graphene owns outstanding electrical performance, while fails in switch control due to its gapless band structure. On the contrary, MoS_2 could realize band engineering with the modulation of its number of layers, whereas its electron mobility is incomparable to that of graphene, making it impossible to act as transparent electrodes [11]. Therefore, fabrication of hybrid structures based on 2D materials by taking advantages of the individual component is one of latest research trends. The ultimate goal is to synthesize more superior composites, achieving synergistic effect or structural reinforcement. This part will focus on the application of MoS_2 based structures both in 2D and 3D areas, including the basic theoretical guidance and synthesis approaches. Finally, the applications of 2D hybrid heterostructures in FET, memory devices, photodetectors, solar cells would be systematically introduced and 3D structures serving as electrodes in HER and lithium ion battery are also covered. Table 2 summarizes the classification and potential applications of 2D van der Waals structures. Table 3 lists the applications of 3D MoS_2 based structures in HER and lithium ion battery. We also give detailed introduction to some of these structures as follows.

4.1. 2D van der Waals heterostructures

Early in 2011, Yandong Ma's group has calculated that the binding energy of per C atom binding to MoS_2 is −23 meV and the forming interlayer spacing between graphene and

Table 1
Summary of the CVD preparation of MoS_2.

Method	Precursor	Growth condition	Morphology	Performance
Sulfurization of Mo based compound	[41] MoO_3, S (180 °C)	Atmosphere, 650 °C	Monolayer	
	[42] MoO_3 nanoribbons, S	850 °C	Monolayer	FET on/off ~6×10^6, mobility ~4.3 cm^2V^{-1} s^{-1}
	[43] MoO_3, S	Atmosphere, 700 °C	Monolayer	FET on/off ~10^5–10^7, mobility ~3–4 cm^2V^{-1} s^{-1}
	[44] MoO_3, S (~100 °C)	~225 mTorr, 530 °C	Monolayer on Mica	Superior optical property
	[38] MoO_3, S (~130 °C)	5 Torr, 670 °C	Monolayer on graphene	10^3 improvement in photoresponse compared to MoS_2
	[39] $MoCl_5$, S	2 Torr, 850 °C	Mono- to few layers on graphene	
Sulfurization of Mo and Mo based oxides	[45] Mo film, S	6.0×10^{-4} mbar, >700 °C	Mono- to few-layers	P-type with an on/off current ratio of ~10^3 and hole mobility up to ~12.2 cm^2V^{-1} s^{-1}
	[46] MoO_2 flakes, S (145 °C)	Atmosphere, 850–950 °C	MoS2 flakes in rhomboid shape	FET on/off 10^4~10^6, mobility 0.1–0.7 cm^2V^{-1} s^{-1}
Thermal decomposition of $(NH_4)_2MoS_4$	[34,47] $(NH_4)_2MoS_4$, S	1–500 Torr, 500–1000 °C	2–3 layers	FET with a low threshold voltage <1 V, high mobility 12.5 cm^2V^{-1} s^{-1}
	[36] $(NH_4)_2MoS_4$	10 mTorr ~ atmosphere, 400 °C	Few layers on graphene	

Table 2
Classification and introduction to the applications of 2D van der Waals structures (graphene: Gr).

Device	MX_2	Method	Structure	Mechanism	Performance
FET	[52] MoS_2	Mechanical exfoliation	MoS_2-Gr	Heterostructure	Current on/off ~36
Memory device	[53] MoS_2	Mechanical exfoliation	MoS_2-Gr	Heterostructure	10^4 difference between memory program and erase states
	[54] MoS_2	Mechanical exfoliation	Gr- MoS_2	Heterostructure	Responsivity 1×10^{10} A/W (130 K)
Photodetector	[55] MoS_2	Mechanical exfoliation	MoS_2 (chemical doping)	p-n junction	EQE ~7000%; specific detectivity ~5×10^{10} J; light switching ratio ~10^3
	[56] MoS_2, WS_2	Mechanical exfoliation	MoS_2-WS_2	Heterostructure	Vertical transistor: photoswitching Ratio 10^3; planar device: ON/OFF ratio >10^5, electron mobility 65 cm^2V^{-1} s^{-1}, photoresponsivity 1.42 A/W
	[57] MoS_2	Mechanical exfoliation	n_Si− MoS_2	n-n junction	Photoresponsivity 7.2 A/W
	[58] MoS_2	Mechanical exfoliation, CVD	Gr- MoS_2	Heterostructure	Responsivity 0~10^4 mA/W
	[59] MoS_2	CVD	Au− MoS_2	Heterostructure	Broadband gain 13.3; detectivity ~10^{10} cm $Hz^{1/2}$/W; photoresponse rise time ~70 μs, fall time ~110 μs; 2 nm device responsivity 0.57 A/W (532 nm) ; working temperature of up to 200 °C
	[60] MoS_2	CVD	Black P− MoS_2	p-n junction	Photodetection responsivity 418 mA/W (633 nm)
Photovoltaic device	[61] MoS_2	Mechanical exfoliation	Au− MoS_2−Au Pd− MoS_2−Pd Pd− MoS_2−Au	Schottky junction	Pd− MoS_2−Au device $V_{oc} = 0.1$ V
	[62] MoS_2	Mechanical exfoliation	Gr- MoS_2- Gr	Heterostructure	EQE 55%; IQE 85%
	[63] MoS_2	Mechanical exfoliation	MoS_2-p_Si	Heterostructure	EQE 4%
	[64] WSe_2, MoS_2	WSe_2: CVD; MoS_2 mechanical exfoliation	WSe_2−MoS_2	p-n junction	Ideality factor 1.2 ; EQE 12%
	[65] MoS_2, WSe_2	Mechanical exfoliation	Gr-MoS_2-WSe_2- Gr	p-n junction	Max EQE 34% (532 nm)
	[66] MoS_2, WSe_2	Mechanical exfoliation	MoS_2−WSe_2	Typellheterostructure	EQE ~1.5%; PCE ~0.2%
	[67] MoS_2	CVD	ITO- MoS_2−Au	Schottky junction	PCE: 1.8% (220 nm MoS_2)
	[60] MoS_2	CVD	Black P−MoS_2	p-n junction	EQE 0.3%

MoS_2 is 3.32 Å. Due to the variation of on-site energy induced by MoS_2, band structure of graphene could be largely preserved in this hybrid structure while introducing a small bandgap of 2 meV which was almost negligible [49]. Further analysis indicated that this band gap was tunable by varying the interlayer spacing, highlighting the prospect in designing of devices with tunable bandgap and high electron mobility simultaneously. In 2011, A. K. Geim proposed "van der Waals heterostructures" on Nature (Fig. 4a) [12], showing a landscape for future development of 2D hybrid structures. Many

Table 3
Applications of 3D MoS_2 based structures in HER and lithium ion battery (graphene: Gr).

Applications	Structure	Method	Performance
HER	[72] MoS_2/carbon nanofiber	Template-directing CVD	Overpotential ~0.12 V, Tafel slope 45 mV/dec
	[73] MoS_2/carbon cloth	Template-directing solvothermal method	Overpotential ~0.15 V, cathodic current density 86 mA/cm^2, Tafel slope 50 mV/dec
	[74] MoS_2/RGO paper	Template-directing solvothermal method	Overpotential ~0.19 V, Tafel slope ~95 mV/dec
	[75] Vertically aligned MoS_2/carbon fiber paper	CVD (MoO_3, S)	Tafel slope 43−47 mV/dec
	[76] MoS_2 nanoparticles/carbon fiber paper	CVD (MoO_3, S)	Overpotential 0.2 V, cathodic current density 200 mA/cm^2, Tafel slope 62 mV/dec
	[77] Vertically aligned MoS_2/carbon nanofiber	CVD (5 nm Mo)	Overpotential −0.3 V, cathodic current density 100 mA/cm^2, Tafel slope 83 mV/dec
Lithium ion battery	[78]MoS_2/Gr	L-cysteine-assisted solution-phase method	100 mA/g current, specific capacity 1100 mAh/g, no capacity fading after 100 cycles
	[15] Honeycomb-like MoS_2/Graphene Foam	Template-directing solvothermal method	BET: 182 m^2/g; 200 mA/g current density, discharge capacity 1235.3 mAh/g; 85.8% retaining of the initial reversible capacity after 60 cycles
	[79] MoS_2 microspheres	Template-directing solvothermal method	100 mA/g current, specific capacity 672 mAh/g after 50 cycles
	[80] MoS_2/CNT	Glucose-assisted hydrothermal method	100 mA/g current rate, capacity 698 mAh/g after 60 cycles
	[81] MoS_2/Gr	Solution phase method	1000 mA/g current density, specific capacity 1040 mAh/g after 50 cycles

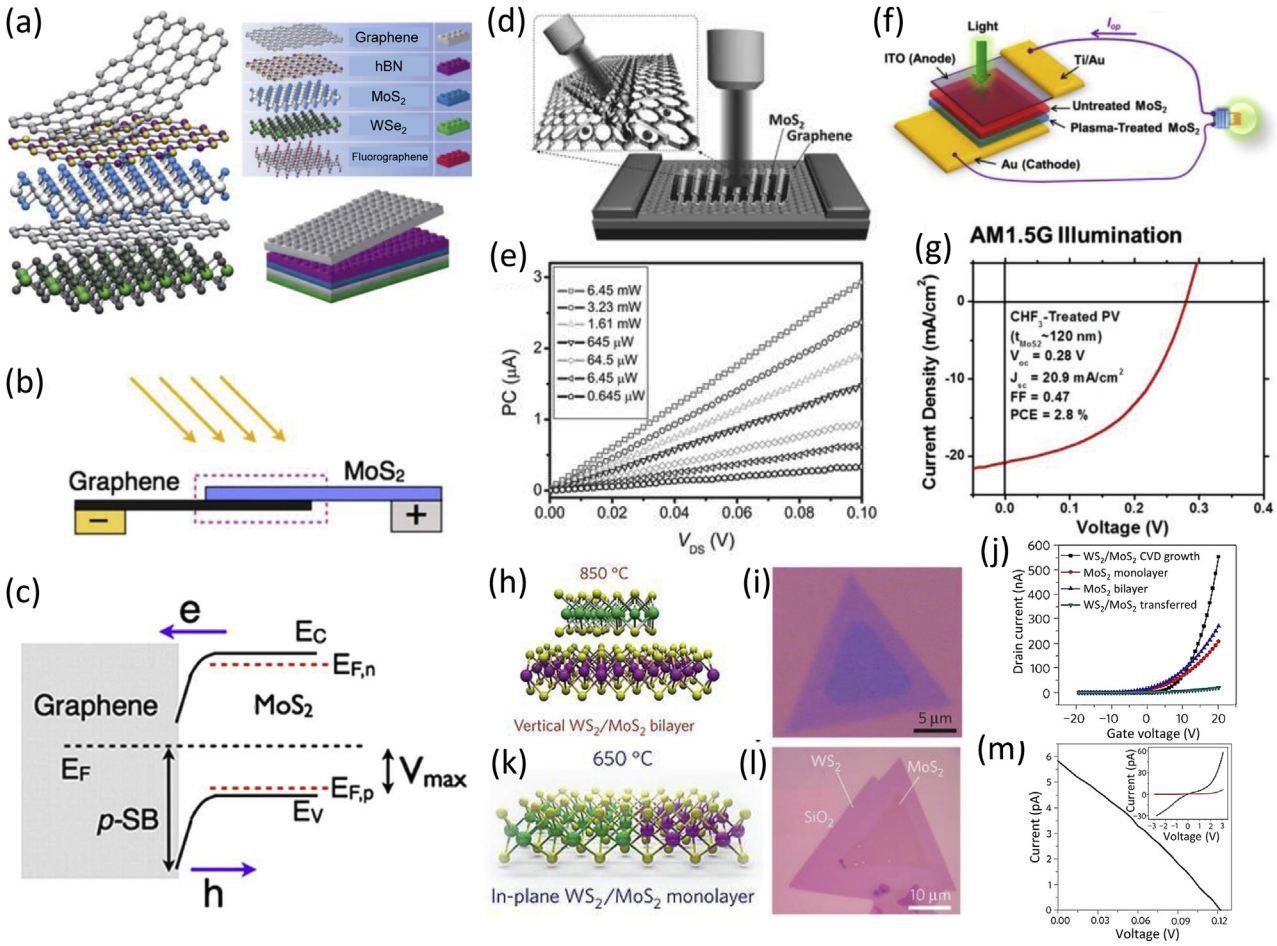

Fig. 4. 2D van der Waals heterostructures. (a) Schematic illustrations of Lego-like van der Waals heterostructures design and construction based on 2D layered materials. (b) MoS_2/graphene interface and Schottky barrier solar cell. M1 and M2 are low and high work function metals respectively. (c) Band alignment at a MoS_2/graphene interface. *p*-SB: hole Schottky barrier; E_f: Fermi energy; E_c: Conduction band bottom; E_v: Valence band top; $E_{F,n}$ and $E_{F,p}$: Quasi-Fermi levels for electrons and holes under illumination; V_{max}: Maximum V_{oc}. (d) Schematic diagram of a graphene-MoS_2 hybrid phototransistor under light irradiation. (e) Photocurrent of the graphene-MoS_2 transistor exhibited in (d) for different optical power as a function of drain-source voltage (V_{DS}). (f) Schematic illustration of the plasma-treated MoS_2 photovoltaic device and (g) *J-V* characteristics measured under illumination of AM1.5 (100 mW/cm^2). (h) Schematic and (i) optical images of the vertically stacked WS_2/MoS_2 heterostructures. (j) Typical plot of gating voltage versus source/drain current of a CVD-grownWS_2/MoS_2 bilayer, a mechanically transferred WS_2/MoS_2 bilayer, a MoS_2 bilayer and monolayer MoS_2. (k) Schematic and (l) optical images of the WS_2/MoS_2 in-plane heterojunctions. (m) Photovoltaic effect of the in-plane heterojunction. Inset is the typical I–V curve of the junction with (black) and without (red) illumination. Panel a reprinted with permission from ref 12. Copyright 2013, Rights Managed by Nature Publishing Group. Panel b, c reprinted with permission from Ref. [50]. Copyright 2013 American Chemical Society. Panel d, e reprinted with permission from Ref. [58]. Copyright 2014 WILEY-VCH Verlag GmbH & Co. KGaA, Weinheim. Panel f, g reprinted with permission from ref 14. Copyright 2014 American Chemical Society. Panel h ~ m reprinted with permission from Ref. [69]. Copyright 2014, Rights Managed by Nature Publishing Group.

challenges were accomplished afterwards, pushing devices into real practical applications. J. C. Grossman and his co-workers confirmed the feasibility by studying the performance of 1 nm-thick solar cell based on MoS_2/graphene through first principles calculations (Fig. 4b, c) [50]. First, MoS_2 like TMDCs monolayers could absorb 5–10% incident sunlight within 1 nm in thickness, exceeding that of traditional semiconductors (GaAs and Si) more than one order of magnitude. In addition, A type-II Schottky junction (Fig. 4c) within 1 nm which would greatly facilitate separation and transport of carriers in the stacking interfaces was constructed, exporting a high power conversion efficiency (PCE) up to ~1%. Moreover, MoS_2/graphene solar cell demonstrated a power density of 0.25–2.5 mW/kg, which were higher by approximately 1–3 orders of magnitude than the best existing ultrathin solar cells [50]. Further experimental observation proved the ultrafast interfacial charge transfer in TMDCs stacking structures, ensuring the effective charge collection and utilization in later circuits [51], opening up the development for light detection and harvesting in atomically thin devices.

Two primary approaches have been adopted to construct devices based on 2D van der Waals heterostructures. One was through layer-by-layer stacking and another was the direct CVD preparation as mentioned above in Part 2. As of layer-by-layer stacking, numerous achievements have been reported. For examples, Hua Xu's group presented a high responsivity 2D graphene-MoS_2 hybrid phototransistor to be continuously tuned from 0~10^4 mA/W by the gate voltage [58]

(Fig. 4d, e). In 2014, Wenjing Zhang's group demonstrated a photodetector with an extremely high photoresponsivity of 10^7 A/W based on graphene- MoS_2, which could achieve a photogain greater than 10^8 [68]. For direct CVD preparation, one breakthrough was proposed by Kathleen M. McCreary and his coworkers, which realized continuous and uniform MoS_2 single-layer films growth on large-area graphene. Recently, P. M. Ajayan's group reported the preparation of both vertically stacked (Fig. 4h, i) and in-plane interconnected WS_2/MoS_2 heterostructures (Fig. 4k, l) through a convenient one-step CVD growth [69]. The vertically stacked layers built a typical type-II band structure, achieving an on/off ratio of up to 10^6 together with the field-effect mobility as high as 15–34 $cm^2/(V \cdot s)$, which exceeded the performance of a mechanically transferred WS_2/MoS_2 bilayer (Fig. 4j) [69]. For the in-plane seamless p-n heterostructures, due to the strong enhancement of localized photoluminescence effect, an open circuit voltage (V_{oc}) of 0.12 V with an short circuit current (I_{sc}) of 5.7 pA could be generated, which exhibited great potential to be used as atomically thin solar cells (Fig. 4m) [69]. Sunjin Wi's group demonstrated MoS_2 based solar cell exhibiting a superior PCE up 2.8% with short circuit current density (J_{sc}) of 20.9 mA/cm^2 (Fig. 4f, g) [14].

4.2. 3D MoS_2 based structures

For 2D heterostructures, the range of applications was mainly focused on electronic and optoelectronic devices. While for applications as supercapacitor, lithium ion battery or HER, design of 3D self-assembled structures were needed generally. The tunable bandgap of MoS_2 indicates they could achieve photoresponsivity over a wide range from ultraviolet to infrared wavelengths with high stability. Moreover, the abundant metallic edges of MoS_2 could facilitate catalytic activity. Besides, MoS_2 with suitable interlayer spacing provides a convenient structure for ions accommodation. Nevertheless, the electrical conductivity and cycling stability of MoS_2 electrodes remain challenging. Fortunately, these two properties could be fully displayed by carbonaceous materials, such as carbon nanotubes (CNT), graphene, or even other organic conducting polymers. They could provide conductive bones for charge separation and transport. Similar to the intention of 2D building blocks design, constructing 3D structures based carbon materials and MoS_2-like TMDCs are of great significance.

The ways to assemble 3D macrostructures include solvothermal synthesis, template-directing method and

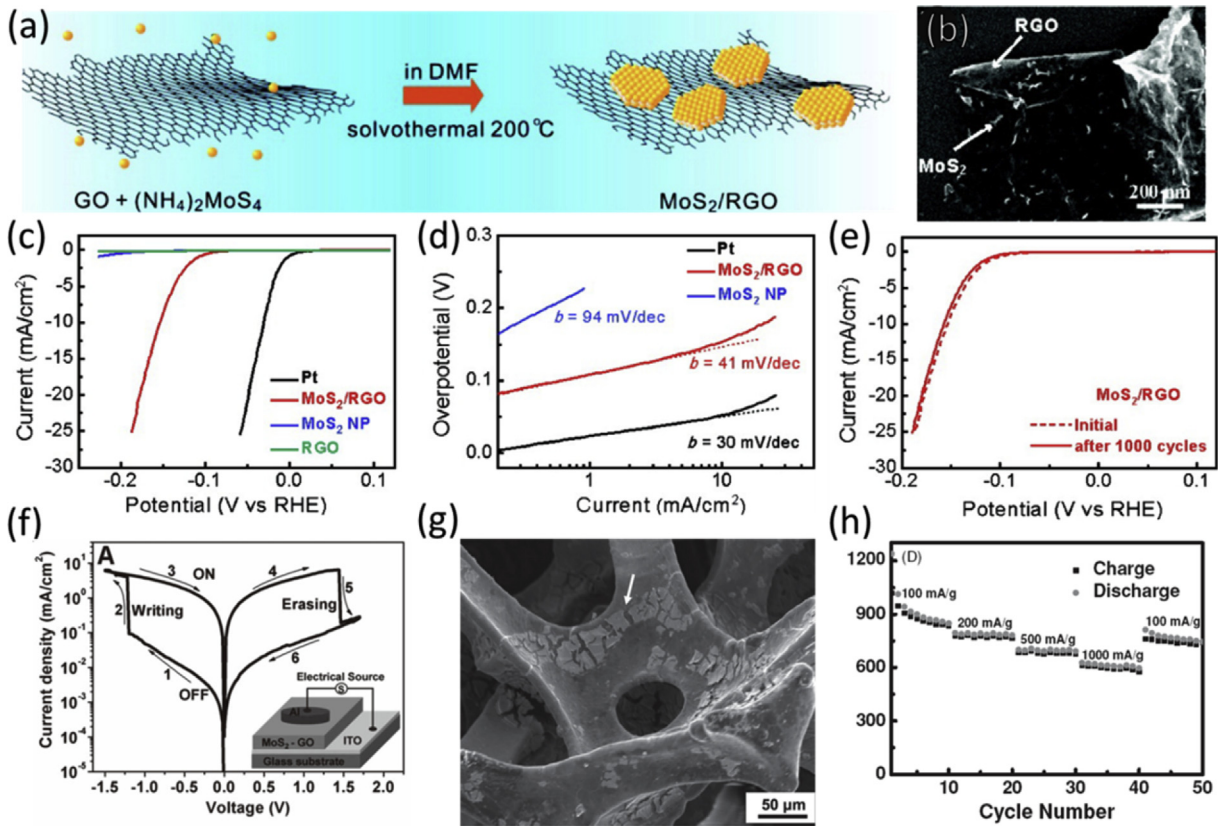

Fig. 5. (a) Schematic solvothermal synthesis and (b) SEM image of the MoS_2/RGO hybrid. (c) Polarization curves (d) corresponding Tafel plots with several catalysts. (e) Durability test for the MoS_2/RGO hybrid catalyst. (f) Typical current density-voltage ($J-V$) plot of an ITO/MoS_2-GO/Al memory device in a "write-read-erase-read" cycle (Inset: schematic structure of the memory device). (g) SEM image and (h) Cycling stability of MoS_2/3D graphene networks composite. Panel a~e reprinted with permission from ref 16. Copyright 2011 American Chemical Society. Panel f reprinted with permission from ref 70. Copyright 2013 WILEY-VCH Verlag GmbH & Co. KGaA, Weinheim. Panel g, h reprinted with permission from Ref. [71]. Copyright 2013 WILEY-VCH Verlag GmbH & Co. KGaA, Weinheim.

combination of both. Till now, MoS_2 and graphene based 3D structures are usually used in the fields of HER and lithium ion battery. Yangguang Li's synthesized MoS_2 nanoparticles on reduced graphene oxide (RGO) sheets through a selective solvothermal method (Fig. 5a, b) [16]. Due to MoS_2's superior electrical coupling to graphene sheets together with its abundant highly exposed edges, the as-prepared MoS_2/RGO hybrid catalyst exhibited competitive HER activity with a small overpotential of ~0.1 V, large cathodic currents and a smaller Tafel slope (41 mV/dec) (Fig. 5c–e) [16]. In 2013, Hua Zhang's group adopted MoS_2-graphene oxide (GO) nanosheets as the active layer for memory devices under low-energy consumption (Fig. 5f) [70]. The MoS_2-GO film based devices showed rewritable nonvolatile memory with low switching voltage of less than 1.5 V and high on/off ratio to be about 10^2. The same group prepared MoS_2-coated 3D graphene networks through CVD method (Fig. 5g) [71]. By taking full advantage of the superior conductivity and high surface area of interconnected 3D graphene networks, together with the excellent electrical contact between MoS_2 and graphene, lithium ion batteries based on this composite displayed reversible capacity of 877 mAh/g at current densities of 100 mA/g during 50th cycle, which achieved enhanced cycling performance than that of simple MoS_2 based devices (Fig. 5h) [71].

5. Conclusion and outlook

After so many years' intensive exploration, graphene-related research has entered into a mature era. However, layered MoS_2 has been triggering a new wave of research and far from being exhausted. Moreover, there exists massive potential to broaden this area by designing and producing 2D or 3D hybrid components by combining graphene and graphene-like 2D blocks. Recently, stable preparation high quality MoS_2 in large area for applications in industrial-scale is still challenging. Research on van der Waals heterostructures reassembling has emerged over the past three years, while the interfacial contact between each building layer needs to be further optimized. In addition, band engineering of both graphene and MoS_2, achieving composite constructions with superior electrical performance and tunable band structure, is a leading topic in the near future. According to the present theoretical basis, many experimental evolutionary results have been obtained at the time of writing. To put the existing flexible optoelectronic and energy storage devices into practical and industrial applications, the most feasible method and technology are needed to be further investigated.

References

[1] Novoselov KS, Geim AK, Morozov SV, Jiang D, Zhang Y, Dubonos SV, et al. Electric field effect in atomically thin carbon films. Science 2004;306:666–9.

[2] Allen MJ, Tung VC, Kaner RB. Honeycomb carbon: a review of graphene. Chem Rev 2010;110:132–45.

[3] Soldano C, Mahmood A, Dujardin E. Production, properties and potential of graphene. Carbon 2010;48:2127–50.

[4] Bae S, Kim H, Lee Y, Xu X, Park JS, Zhang Y, et al. Roll-to-roll production of 30-inch graphene films for transparent electrodes. Nat Nanotechnol 2010;5:574–8.

[5] Zang X, Chen Q, Li P, He Y, Li X, Zhu M, et al. Highly flexible and adaptable, all-solid-state supercapacitors based on graphene woven-fabric film electrodes. Small 2014;10:2583–8.

[6] Li X, Zang X, Li X, Zhu M, Chen Q, Wang K, et al. Hybrid heterojunction and solid-state photoelectrochemical solar cells. Adv Energy Mater 2014;4:1400224.

[7] Li X, Xie D, Park H, Zeng Helen T, Wang K, Wei J, et al. Anomalous behaviors of graphene transparent conductors in graphene-silicon heterojunction solar cells. Adv Energy Mater 2014;3:1029–34.

[8] Wang Y, Wang L, Yang T, Li X, Zang X, Zhu M, et al. Wearable and highly sensitive graphene strain sensors for human motion monitoring. Adv Funct Mater 2014;24:4666–70.

[9] Things you could do with graphene.(a) Ahn JH, Hong BH. Graphene for displays that bend.(b) Torrisi F, Coleman JN. Electrifying inks with 2D materials.(c) Liu J. Charging graphene for energy.(d) Bohm S. Graphene against corrosion.(e) Drndic M. Sequencing with graphene pores.(f) Kostarelos K, Novoselov KS. Graphene devices for life. (g) Siochi EJ. Graphene in the sky and beyond. Nat Nanotechnol 2014;9:737–47.

[10] Ganatra R, Zhang Q. Few-layer MoS_2: a promising layered semiconductor. ACS Nano 2014;8:4074–99.

[11] Chhowalla M, Shin HS, Eda G, Li LJ, Loh KP, Zhang H. The chemistry of two-dimensional layered transition metal dichalcogenide nanosheets. Nat Chem 2014;5:263–75.

[12] Geim AK, Grigorieva IV. van der Waals heterostructures. Nature 2013;499:419–25.

[13] Yu GL, Jalil R, Belle B, Mayorov AS, Blake P, Schedin F, et al. Interaction phenomena in graphene seen through quantum capacitance. PNAS 2013;110:3282–6.

[14] Wi S, Kim H, Chen M, Nam H, Guo LJ, Meyhofer E, et al. Enhancement of photovoltaic response in multilayer MoS_2 induced by plasma doping. ACS Nano 2014;8:5270–81.

[15] Ding S, Zhang D, Chen JS, Lou XW. Facile synthesis of hierarchical MoS_2 microspheres composed of few-layered nanosheets and their lithium storage properties. Nanoscale 2012;4:95–8.

[16] Li Y, Wang H, Xie L, Liang Y, Hong G, Dai H. MoS_2 nanoparticles grown on graphene: an advanced catalyst for the hydrogen evolution reaction. J Am Chem Soc 2011;133:7296–9.

[17] Wu W, Wang L, Li Y, Zhang F, Lin L, Niu S, et al. Piezoelectricity of single-atomic-layer MoS_2 for energy conversion and piezotronics. Nature 2014;514:470–4.

[18] Jariwala D, Sangwan VK, Lauhon LJ, Marks TJ, Hersam MC. Emerging device applications for semiconducting two-dimensional transition metal dichalcogenides. ACS Nano 2014;8:1102–20.

[19] Eda G, Yamaguchi H, Voiry D, Fujita T, Chen M, Chhowalla M. Photoluminescence from chemically exfoliated MoS_2. Nano Lett 2011;11:5111–6.

[20] Akinwande D, Petrone N, Hone J. Two-dimensional flexible nanoelectronics. Nat Commun 2014;5(5678):1–12.

[21] Lee C, Yan H, Brus LE, Heinz TF, Hone J, Ryu S. Anomalous lattice vibrations of single and few-layer MoS_2. ACS Nano 2010;4:2695–700.

[22] Zhan Y, Liu Z, Najmaei S, Ajayan PM, Lou J. Large-area vapor-phase growth and characterization of MoS_2 atomic layers on a SiO_2 substrate. Small 2012;8:966–71.

[23] Splendiani A, Sun L, Zhang Y, Li T, Kim J, Chim CY, et al. Emerging photoluminescence in monolayer MoS_2. Nano Lett 2010;10:1271–5.

[24] Radisavljevic B, Radenovic A, Brivio J, Giacometti V, Kis A. Single-layer MoS_2 transistors. Nat Nanotechnol 2011;6:147–50.

[25] Yin Z, Li H, Li H, Jiang L, Shi Y, Sun Y, et al. Single-layer MoS_2 phototransistors. ACS Nano 2012;6:74–80.

[26] Li H, Wu J, Yin Z, Zhang H. Preparation and applications of mechanically exfoliated single-layer and multilayer MoS_2 and WSe_2 nanosheets. Acc Chem Res 2014;47:1067–75.

[27] Gacem K, Boukhicha M, Chen Z, Shukla A. High quality 2D crystals made by anodic bonding: a general technique for layered materials. Nanotechnology 2012;23:505709.

[28] Zeng Z, Yin Z, Huang X, Li H, He Q, Lu G, et al. Single-layer semiconducting nanosheets: high-yield preparation and device fabrication. Angew Chem Int Ed 2011;50:11093–7.

[29] Coleman JN, Lotya M, O'Neill A, Bergin SD, King PJ, Khan U, et al. Two-dimensional nanosheets produced by liquid exfoliation of layered materials. Science 2011;331:568–71.

[30] O'Neill A, Khan U, Coleman JN. Preparation of high concentration dispersions of exfoliated MoS_2 with increased flake size. Chem Mater 2012;24:2414–21.

[31] Lee YH, Zhang XQ, Zhang W, Chang MT, Lin CT, Chang KD, et al. Synthesis of large-area MoS_2 atomic layers with chemical vapor deposition. Adv Mater 2012;24:2320–5.

[32] Yu Y, Li C, Liu Y, Su L, Zhang Y, Cao L. Controlled scalable synthesis of uniform, high-quality monolayer and few-layer MoS_2 films. Sci Rep 2013;3(1866):1–6.

[33] Lin YC, Zhang W, Huang JK, Liu KK, Lee YH, Liang CT, et al. Wafer-scale MoS_2 thin layers prepared by MoO_3 sulfurization. Nanoscale 2012;4:6637–41.

[34] Liu KK, Zhang W, Lee YH, Lin YC, Chang MT, Su CY, et al. Growth of large-Area and highly crystalline MoS_2 thin layers on insulating substrates. Nano Lett 2012;12:1538–44.

[35] Wu S, Huang C, Aivazian G, Ross JS, Cobden DH, Xu X. Vapor solid growth of high optical quality MoS_2 monolayers with near-unity valley polarization. ACS Nano 2013;7:2768–72.

[36] Shi Y, Zhou W, Lu AY, Fang W, Lee YH, Hsu AL, et al. van der Waals epitaxy of MoS_2 layers using graphene as growth templates. Nano Lett 2012;12:2784–91.

[37] Duan X, Wang C, Shaw JC, Cheng R, Chen Y, Li H, et al. Lateral epitaxial growth of two-dimensional layered semiconductor heterojunctions. Nat Nanotechnol 2014;9:1024–30.

[38] Lin YC, Lu N, Perea-Lopez N, Li J, Lin Z, Peng X, et al. Direct synthesis of van der Waals solids. ACS Nano 2014;8:3715–23.

[39] McCreary KM, Hanbicki AT, Robinson JT, Cobas E, Culbertson JC, Friedman AL, et al. Large-area synthesis of continuous and uniform MoS_2 monolayer films on graphene. Adv Funct Mater 2014;24:6449–54.

[40] Shi Y, Li H, Li LJ. Recent advances in controlled synthesis of two-dimensional transition metal dichalcogenides via vapour deposition techniques. Chem Soc Rev 2015. http://dx.doi.org/10.1039/C4CS00256C.

[41] Ling X, Lee YH, Lin Y, Fang W, Yu L, Dresselhaus MS, et al. Role of the seeding promoter in MoS_2 growth by chemical vapor deposition. Nano Lett 2014;1:464–72.

[42] Najmaei S, Liu Z, Zhou W, Zou X, Shi G, Lei S, et al. Vapour phase growth and grain boundary structure of molybdenum disulphide atomic layers. Nat Mater 2013;12:754–9.

[43] Van der Zande AM, Huang PY, Chenet DA, Berkelbach TC, You YM, Lee GH, et al. Grains and grain boundaries in highly crystalline monolayer molybdenum disulphide. Nat Mater 2013;12:554–61.

[44] Ji Q, Zhang Y, Gao T, Zhang Y, Ma D, Liu M, et al. Epitaxial monolayer MoS_2 on mica with novel photoluminescence. Nano Lett 2013;13:3870–7.

[45] Tao J, Chai JW, Lu X, Wong LM, Wong TI, Pan J, et al. Growth of waferscale MoS_2 monolayer by magnetron sputtering. Nanoscale 2015;7:2497–503. http://dx.doi.org/10.1039/C4NR06411A.

[46] Wang X, Feng H, Wu Y, Jiao L. Controlled synthesis of highly crystalline MoS_2 flakes by chemical vapor deposition. J Am Chem Soc 2013;135:5304–7.

[47] Pu J, Yomogida Y, Liu KK, Li LJ, Iwasa Y, Takenobu T. Highly flexible MoS_2 thin-film transistors with ion gel dielectrics. Nano Lett 2012;12:4013–7.

[48] Wang H, Liu F, Fang Z, Zhou W, Liu Z. Two-dimensional heterostructures: fabrication, characterization, and application. Nanoscale 2014;6:12250–72.

[49] Ma Y, Dai Y, Guo M, Niu C, Huang B. Graphene adhesion on MoS_2 monolayer: an ab initio study. Nanoscale 2011;3:3883–7.

[50] Bernardi M, Palummo M, Grossman JC. Extraordinary sunlight absorption and one nanometer thick photovoltaics using two-dimensional monolayer materials. Nano Lett 2013;13:3664–70.

[51] Hong X, Kim J, Shi SF, Zhang Y, Jin C, Sun Y, et al. Ultrafast charge transfer in atomically thin MoS_2/WS_2 heterostructures. Nat Nanotechnol 2014;9:682–6.

[52] Shih CJ, Wang QH, Son Y, Jin Z, Blankschtein D, Strano MS. Tuning on-off current ratio and field-effect mobility in a MoS_2-graphene heterostructure via Schottky barrier modulation. ACS Nano 2014;8:5790–9.

[53] Bertolazzi S, Krasnozhon D, Kis A. Nonvolatile memory cells based on MoS_2/graphene heterostructures. ACS Nano 2013;7:3246–52.

[54] Roy K, Padmanabhan M, Goswami S, Sai TP, Ramalingam G, Raghavan S, et al. Graphene-MoS_2 hybrid structures for multifunctional photoresponsive memory devices. Nat Nanotechnol 2013;8:826–30.

[55] Choi MS, Qu D, Lee D, Liu X, Watanabe K, Taniguchi T, et al. Lateral MoS_2 p-n junction formed by chemical doping for use in high-performance optoelectronics. ACS Nano 2014;8:9332–40.

[56] Huo N, Kang J, Wei Z, Li SS, Li J, Wei SH. Novel and enhanced optoelectronic performances of multilayer MoS_2-WS_2 heterostructure transistors. Adv Funct Mater 2014;24:7025–31.

[57] Li Y, Xu CY, Wang JY, Zhen L. Photodiode-like behavior and excellent photoresponse of vertical Si/monolayer MoS_2 heterostructures. Sci Rep 2014;4(7186):1–8.

[58] Xu H, Wu J, Feng Q, Mao N, Wang C, Zhang J. High responsivity and gate tunable graphene-MoS_2 hybrid phototransistor. Small 2014;10:2300–6.

[59] Tsai DS, Liu KK, Lien DH, Tsai ML, Kang CF, Lin CA, et al. Few-layer MoS_2 with high broadband photogain and fast optical switching for use in harsh environments. ACS Nano 2013;7:3905–11.

[60] Deng Y, Luo Z, Conrad NJ, Liu H, Gong Y, Najmaei S, et al. Black phosphorus-monolayer MoS_2 van der Waals heterojunction p-n diode. ACS Nano 2014;8:8292–9.

[61] Fontana M, Deppe T, Boyd AK, Rinzan M, Liu AY, Paranjape M, et al. Electron-hole transport and photovoltaic effect in gated MoS_2 Schottky junctions. Sci Rep 2013;3(1634):1–5.

[62] Yu WJ, Liu Y, Zhou H, Yin A, Li Z, Huang Y, et al. Highly efficient gate-tunable photocurrent generation in vertical heterostructures of layered materials. Nat Nanotechnol 2013;8:952–8.

[63] Lopez-Sanchez O, Alarcon Llado E, Koman V, Fontcuberta i Morral A, Radenovic A, Kis A. Light generation and harvesting in a van der Waals heterostructure. ACS Nano 2014;8:3042–8.

[64] Cheng R, Li D, Zhou H, Wang C, Yin A, Jiang S, et al. Electroluminescence and photocurrent generation from atomically sharp WSe_2/MoS_2 heterojunction p-n diodes. Nano Lett 2014;14:5590–7.

[65] Lee CH, Lee GH, van der Zande AM, Chen W, Li Y, Han M. Atomically thin p-n junctions with van der Waals heterointerfaces. Nat Nanotechnol 2014;9:676–81.

[66] Furchi MM, Pospischil A, Libisch F, Burgdörfer J, Mueller T. Photovoltaic effect in an electrically tunable van der Waals heterojunction. Nano Lett 2014;14:4785–91.

[67] Shanmugam M, Durcan CA, Yu B. Layered semiconductor molybdenum disulfide nanomembrane based Schottky-barrier solar cells. Nanoscale 2012;4:7399–405.

[68] Zhang W, Chuu CP, Huang JK, Chen CH, Tsai ML, Chang YH, et al. Ultrahigh-gain photodetectors based on atomically thin graphene-MoS_2 heterostructures. Sci Rep 2014;4(3826):1–8.

[69] Gong Y, Lin J, Wang X, Shi G, Lei S, Lin Z, et al. Vertical and in-plane heterostructures from WS_2/MoS_2 monolayers. Nat Mater 2014;13:1135–42.

[70] Yin Z, Zeng Z, Liu J, He Q, Chen P, Zhang H. Memory devices using a mixture of MoS_2 and graphene oxide as the active layer. Small 2013;9:727–31.

[71] Cao X, Shi Y, Shi W, Rui X, Yan Q, Kong J, et al. Preparation of MoS_2-coated three-dimensional graphene networks for high-performance anode material in lithium-ion batteries. Small 2013;9:3433–8.

[72] Zhu H, Du ML, Zhang M, Zou M, Yang T, Fu Y, et al. The design and construction of 3D rose-petal-shaped MoS_2 hierarchical nanostructures with structure-sensitive properties. J Mater Chem A 2014;2:7680–5.

[73] Ma CB, Qi X, Chen B, Bao S, Yin Z, Wu XJ, et al. MoS_2 nanoflower-decorated reduced graphene oxide paper for high-performance hydrogen evolution reaction. Nanoscale 2014;6:5624–9.

[74] Yan Y, Xia BY, Li N, Xu ZC, Fisherc A, Wang X. Vertically oriented MoS_2 and WS_2 nanosheets directly grown on carbon cloth as efficient and stable 3-dimensional hydrogen-evolving cathodes. J Mater Chem A 2015;3:131–5.
[75] Wang H, Lu Z, Xu S, Kong D, Cha JJ, Zheng G, et al. Electrochemical tuning of vertically aligned MoS_2 nanofilms and its application in improving hydrogen evolution reaction. PNAS 2013;110:19701–6.
[76] Wang H, Lu Z, Kong D, Sun J, Hymel TM, Cui Y. Electrochemical tuning of MoS_2 nanoparticles on three-dimensional substrate for efficient hydrogen evolution. ACS Nano 2014;8:4940–7.
[77] Wang H, Zhang Q, Yao H, Liang Z, Lee HW, Hsu PC, et al. High electrochemical selectivity of edge versus terrace sites in two-dimensional layered MoS_2 materials. Nano Lett 2014;14:7138–44.
[78] Chang K, Chen W. L-cysteine-assisted synthesis of layered MoS_2/graphene composites with excellent electrochemical performances for lithium ion batteries. ACS Nano 2011;5:4720–8.
[79] Zhang X, Luster B, Church A, Muratore C, Voevodin AA, Kohli P, et al. Carbon nanotube–MoS_2 composites as solid lubricants. ACS Appl Mater Interf 2009;1:735–9.
[80] Ding S, Chen JS, Lou XWD. Glucose-assisted growth of MoS_2 nanosheets on CNT backbone for improved lithium storage properties. Chem A Eur J 2011;17:13142–5.
[81] Chang K, Chen W. In situ synthesis of MoS_2/graphene nanosheet composites with extraordinarily high electrochemical performance for lithium ion batteries. Chem Commun 2011;47:4252–4.

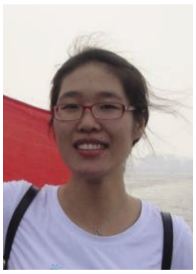

Xiao Li is a PhD student of Materials Science of School of Materials Science and Engineering, Tsinghua University, Beijing, China. She obtained her Bachelor's Degree in 2011 from the College of Mechanical and Electronic Engineering, China University of Petroleum, China. Her research interests focus on the preparation and applications of two-dimensional materials, with an emphasis on graphene and metal dichalcogenides.

Dr. Hongwei Zhu is a Professor of Materials Science of School of Materials Science and Engineering, Tsinghua University, Beijing, China. Before joining the faculty of Tsinghua University in 2008, he had conducted Post Doc. studies in Japan and USA since 2003. His recent research focuses on macrostructural assembly and engineering of nanomaterials (*e.g.*, graphene and carbon nanotubes), flexible energy devices, sensors, and membranes for water desalination and purification. He has published over 160 papers in refereed international journals, 2 books and 5 invited book chapters, and holds 12 Chinese patents and 1 US patent.